24th COBEM - 2017

24th ABCM International Congress of Mechanical Engineering
December 3-8, 2017, Curitiba, PR, Brazil

COBEM-2017-1937
ANALYSIS OF A DYNAMIC SYSTEM SUBJECTED TO AN IMPULSIVE AND INTERNAL CONTACT FORCE

Gustavo Simão Rodrigues
Hans Ingo Weber
Pontifícia Universidade Católica. Rio de Janeiro, RJ, Brazil
simao@ime.eb.br
hans@puc-rio.br

Abstract. *Many industrial equipment assemblies present internal impacts during operation. The impact and impulsive forces are characterized by large amplitude of force in a very short period of time. An example of equipment subjected to an impulsive force is the recoil mechanism of an armament. The recoil mechanism moderates the firing loads exerted on the armature support structure by prolonging the resistance time of the forces generated by the propellant gases. Basically, the recoil mechanism can be simplified by a spring-damper connected to the barrel to cushion the force exerted on the breech. This paper analyses a simplified recoil mechanism and two new models to improve the barrel response in terms of maximum displacement.*

Keywords: *Recoil Mechanism; Impulsive Forces; Dynamic Systems.*

1. INTRODUCTION

The first known recoil system dates back to the late 19th century, equipping a 75 mm French caliber called "Matériel de 75mm Mle 1897", commonly called French 75 or simply 75 (Hallenberg, 2006). At that time, the revolutionary recoil system was a hydropneumatic type and allowed the tube to retreat while its support remained static on the ground. After the tube retracted, the system moved it forward to the firing position.

Some authors discuss methods to model the recoil system. Lin et. al. (2009) suggest two different kind of methods. Tiwari et. al. (2016) deal with rigid body dynamic modeling for a representative howitzer system. Hassanan (2014a), Hassanan (2014b) and Hassanan (2014c) present variations in the model of pneumatic recoil system and in the coefficient of the hydraulic damper.

2. METHODOLOGY

A recoil mechanism can be represented by a simplified model as shown in Fig. 1. It consists in a barrel with mass M where the degree of freedom is x_M. In one extremity of the barrel is applied an impulsive force $F(t)$ and at the other extremity the links are effectuated by a spring with stiffness k and a damper with damping coefficient c.

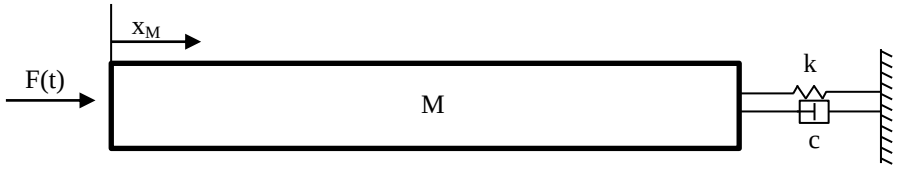

Figure 1. Simplified model of a recoil mechanism

The new proposed models intended to improve the recoil mechanism are presented in Fig. 2 and Fig. 3. A system with mass m is attached to the tube in model (i). In model (ii), the mass m is attached to the ground. In both models, the degree of freedom that describes the motion of this mass m is x_m. Mass m can slide frictionless horizontally and is at a distance, namely the gap, of one end of the wall, namely A. At the other end, the mass m is connected to an actuator that reproduces a spring-damper with variable stiffness and damping coefficients k_r and c_r. An impulsive force $F(t)$ is applied to the mass barrel M which starts the device.

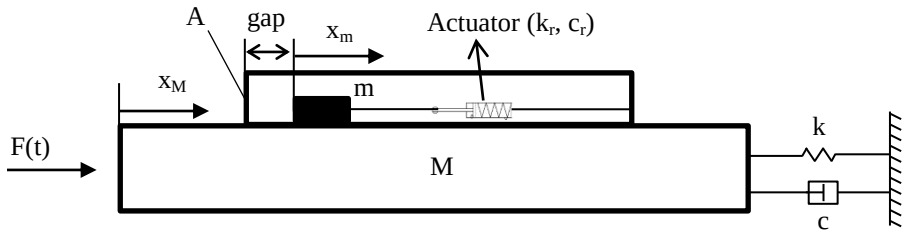

Figure 2. New proposed model (i)

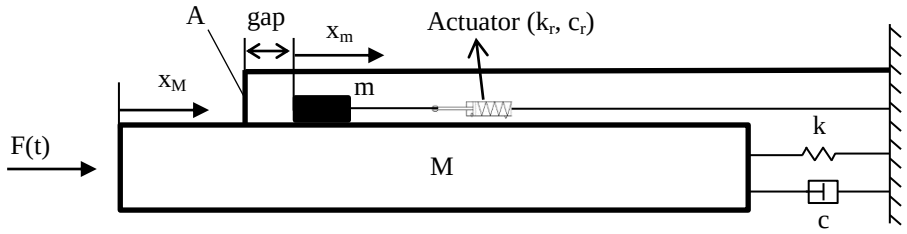

Figure 3. New proposed model (ii)

2.1 Maximum Displacement Analisys

The impulsive force *F(t)* can be replaced by an initial velocity (v_0) of mass *M* which equation of motion is shown in Eq. (1):

$$\mathrm{M}\ddot{\mathrm{x}}_\mathrm{M} + \mathrm{k}\mathrm{x}_\mathrm{M} + \mathrm{c}\dot{\mathrm{x}}_\mathrm{M} = 0. \tag{1}$$

The damping coefficient *c* is considered as (Polach and Hajžman, 2010)

$$\mathrm{c} = 6239\ \mathrm{N{\cdot}s/m\ if}\ \dot{\mathrm{x}}_\mathrm{M} > 0 \tag{2}$$

and

$$\mathrm{c} = 14050\ \mathrm{N{\cdot}s/m\ if}\ \dot{\mathrm{x}}_\mathrm{M} < 0. \tag{3}$$

The stiffness coefficient *k* is considered as 27500 N/m and the initial conditions are $\mathrm{x_M} = 0$ and $\dot{\mathrm{x}}_\mathrm{M} = v_0$. The initial velocity v_0 can be found by conservation of momentum considering the integral in time of the impulsive force. The mass of the projectile is considered as 6.86 kg, the mass of the tube *M* is 5600 kg and the velocity of the projectile after the firing is equal to 564 m/s. Thus, v_0 is 0.7 m/s. (Hassaan, 2014a)

Model (i) equations of motion are presented in Eq. (4) and Eq. (5). It should be noted that mass *m* must be considered for the equation of motion the tube of mass *M* since the system with actuator is embarked in the tube. This will affect the initial velocity of the mass *M*. Besides there is also a contact force, F_{ct}, due to the contact between the mass *m* and the wall *A* of the actuator system, which is considered integral with the tube of mass *M*.

$$\mathrm{M}\ddot{\mathrm{x}}_\mathrm{M} + \mathrm{k}\mathrm{x}_\mathrm{M} + \mathrm{c}\dot{\mathrm{x}}_\mathrm{M} + (\dot{\mathrm{x}}_\mathrm{M} - \dot{\mathrm{x}}_\mathrm{m})\mathrm{c}_\mathrm{r} + (\mathrm{x}_\mathrm{M} - \mathrm{x}_\mathrm{m})\mathrm{k}_\mathrm{r} - \mathrm{F}_\mathrm{ct} = 0 \tag{4}$$

$$\mathrm{m}\ddot{\mathrm{x}}_\mathrm{m} - (\dot{\mathrm{x}}_\mathrm{M} - \dot{\mathrm{x}}_\mathrm{m})\mathrm{c}_\mathrm{r} - (\mathrm{x}_\mathrm{M} - \mathrm{x}_\mathrm{m})\mathrm{k}_\mathrm{r} + \mathrm{F}_\mathrm{ct} = 0 \tag{5}$$

The contact force, F_{ct}, used is similar to the model proposed by Hunt and Crossley (1975) and exposed in Eq. (6):

$$\mathrm{F}_{ct}(\delta, \dot{\delta}) = -k_c\delta^{n_c} - c_c\delta^{n_c}\dot{\delta} = -k_c\delta^{n_c}(1 + \lambda_\mathrm{c}\dot{\delta}), \text{ with } \lambda_\mathrm{c} = \frac{c_c}{k_c} \tag{6}$$

where δ is the deformation of the contact region defined as $x_m - (x_M + gap)$, $\dot{\delta}$ is the deformation velocity, i.e., $\dot{\delta} = (\dot{\mathrm{x}}_\mathrm{m} - \dot{\mathrm{x}}_\mathrm{M})$, k_c is the contact stiffness, c_c is the viscous damping and λ_c a coefficient of proportionality. The exponent n_c depends on the geometric characteristics around the contact surface. The initial conditions of Eq. (4) and Eq. (5) are: $\mathrm{x_M}(0) = 0$, $\dot{\mathrm{x}}_\mathrm{M}(0) = \mathrm{v}_0$, $\mathrm{x_m}(0) = 0$, $\dot{\mathrm{x}}_\mathrm{m}(0) = 0$.

It should be noted that the contact force F_{ct} will only act on the system when the values δ and $\dot{\delta}$ are negative. For δ> 0, the contact force F_{ct} is zero, i.e., there is no contact between the mass *m* and the wall *A* of the system.

The parameters used to simulate the contact force are similar to the values used by Aguiar (2006). In addition to these, other parameters are listed in Tab. 1.

Table 1. Values used for actuator system in models (i) and (ii)

Parameter	**Value**
Stiffness (k_c)	$2.1 \cdot 10^8$ N/m
Factor of non-linearity (n_c)	1.3
Coefficient of proportionality (λ_c)	0.6
k_r	13500 N/m
c_r	3675 N·s/m

The equations of motion for the system with an actuator, model (ii), are presented in Eq. (7) and Eq. (8).

$$M\ddot{x}_M + kx_M + c\dot{x}_M - F_{ct} = 0 \tag{7}$$

$$m\ddot{x}_m + k_r x_m + c_r \dot{x}_m + F_{ct} = 0 \tag{8}$$

The initial conditions and the contact force, F_{ct}, are similar to those discussed for the system of equations presented in Eq. (4) and Eq. (5).

The maximum displacements of mass *M* for models (i) and (ii) are shown in Fig. 4 and Fig. 5, respectively, for a gap variation from 0 to a maximum value and for some mass *m*. It is worth remembering that the objective is to analyze the displacement of the mass *M* and this value is observed in the axis of the ordinates in Fig. 4 and Fig 5.

The new proposed models represent a two degree of freedom system and with a peculiarity of the existence of an impact force between mass *m* and the wall *A*. Depending on the values of mass *m* and the gap, we will have different system responses in terms of maximum displacement of mass *M*. Considering model (i), Fig. 4 shows the maximum displacement of mass *M* for different values of mass *m* and sweeping the gap from zero, i. e., mass *m* in contact with wall *A*, until the gap of 120 mm.

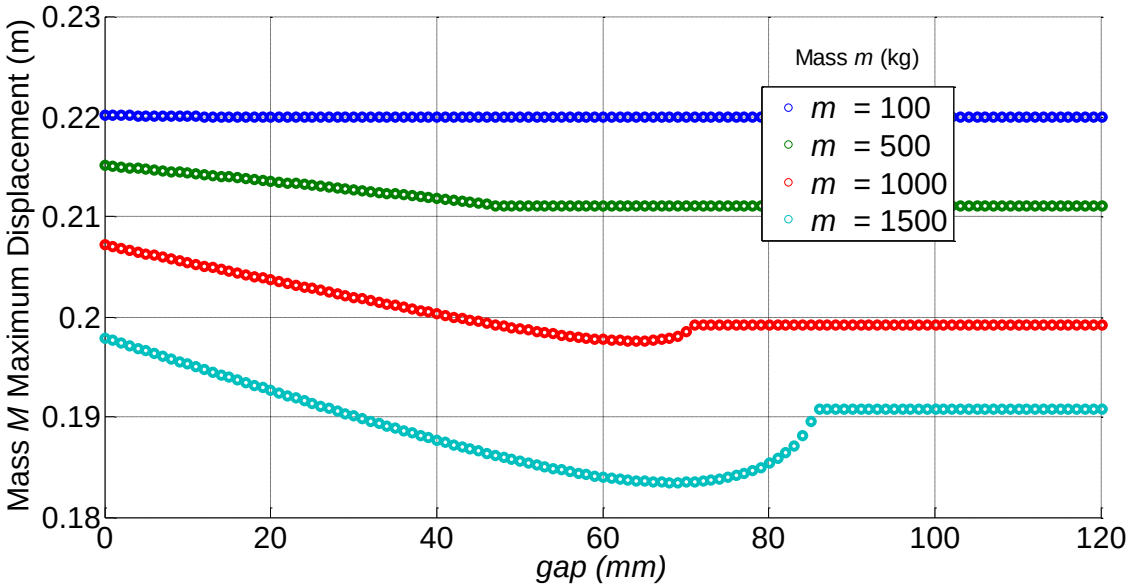

Figure 4. Maximum displacement of mass *M* varying mass *m* and the gap. Model (i)

When we analyze model (ii), the maximum displacement of mass *M* for different values of mass *m* and the gap is presented in Fig. 5, concluding that the maximum displacement of mass *M* takes place when the gap is zero.

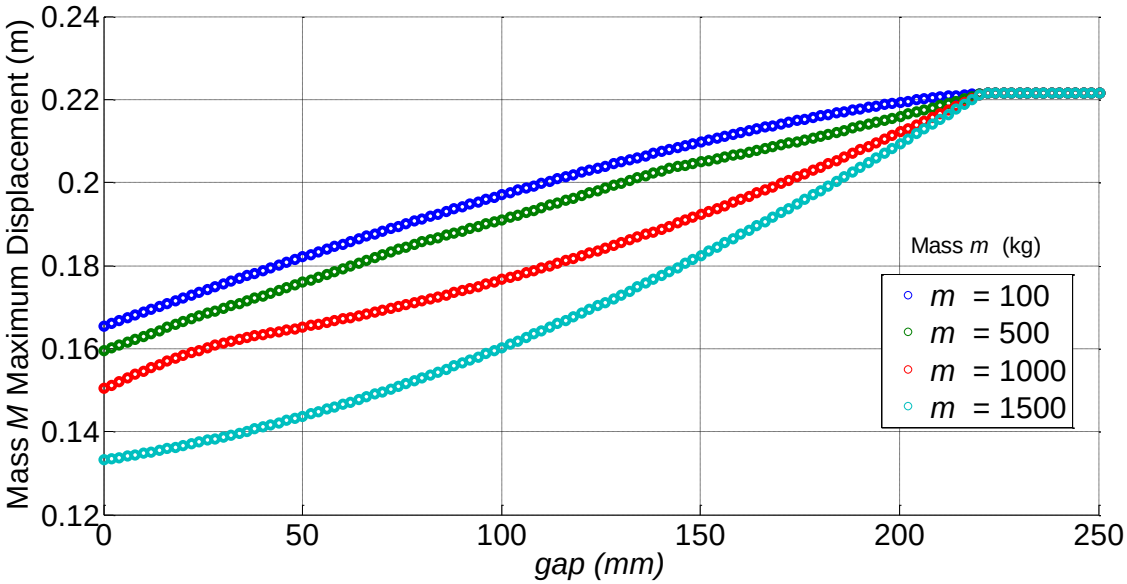

Figure 5. Maximum displacement of mass *M* varying mass *m* and the gap. Model (ii)

In Fig 6, the Simplified Model, model (i) and model (ii) are compared for gap equal to zero and mass *m* equal to 100 kg in terms of maximum mass *M* displacements. The difference between the Simplified Model and model (i) is negligible and a relatively lower value of maximum mass *M* displacement for model (ii) is observed.

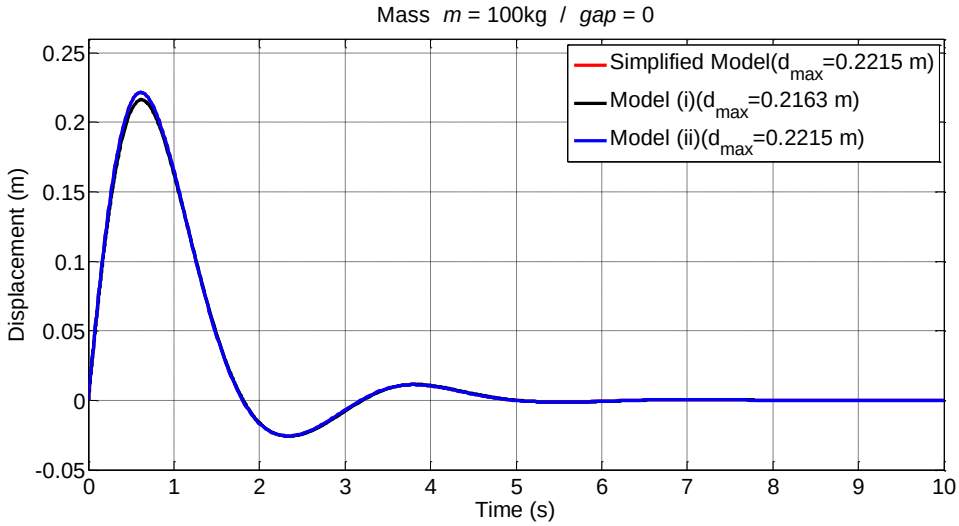

Figure 6. Maximum displacement of mass M (*m* = 100 kg)

As mass *m* increases, the difference between the maximum displacement of mass *M* in the Simplified Model and model (i) increases, as can be seen in Fig. 7 and Fig 8. Note that the maximum displacement of mass *M* in model (ii) also suffers considerable reduction when mass *m* is increased.

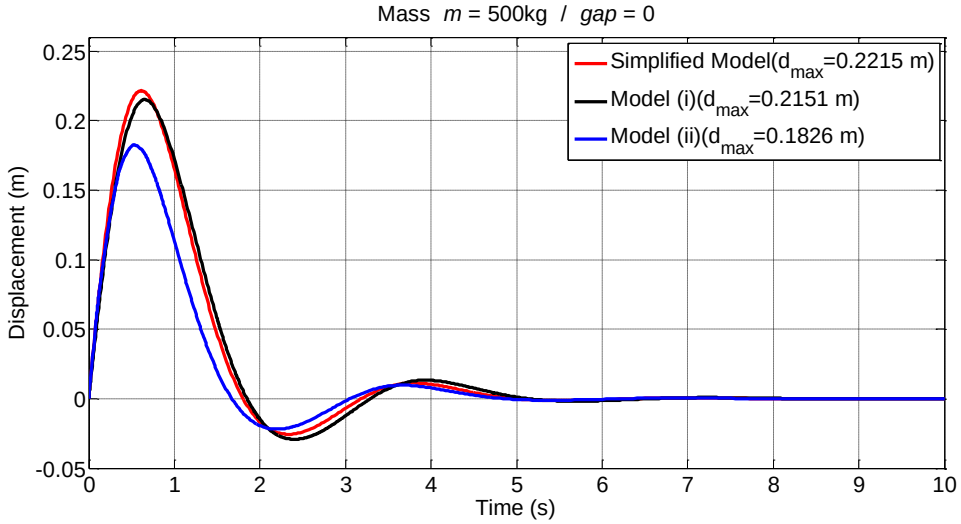

Figure 7. Maximum displacement of mass M (m = 500 kg)

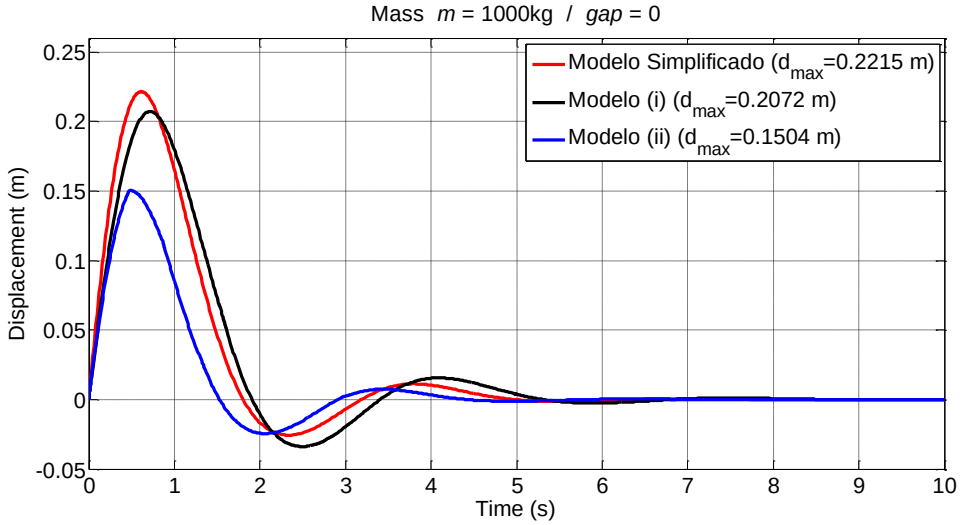

Figure 8. Maximum displacement of mass M (m = 1000 kg)

Table 2 summarizes the values of the maximum displacements of mass M found in the above graphs for the three models analyzed.

Table 2. Summary of maximum displacement of mass M

	Maximum mass M displacements		
Mass m	100 kg	500 kg	1000 kg
Simplified Model	0.2215 m	0.2215 m	0.2215 m
Model (i)	0.2163 m	0.2151 m	0.2072 m
Model (ii)	0.2215m	0.1826 m	0.1504 m

2.2 Contact Force Analysis

The impact between mass m and wall A causes sudden changes in the velocity of mass m. These changes of velocity are evaluated by the contact force, F_{ct}, existing in models (i) and (ii), as can be seen in Eq. (5) and Eq. (7).

Figure 9 shows the contact force profiles for model (i) (Fig. 9a) and model (ii) (Fig 9c) and also the details for the main effective impacts for model (i)) (Fig. 9b) and model (ii) (Fig 9d).

One can observe that the peak force for model (i) 114.4 kN. is and for model (ii) is 116.7 kN, i.e., a small difference of maximum forces. However, the following peaks of the impact force of model (i) are substantially smaller than the

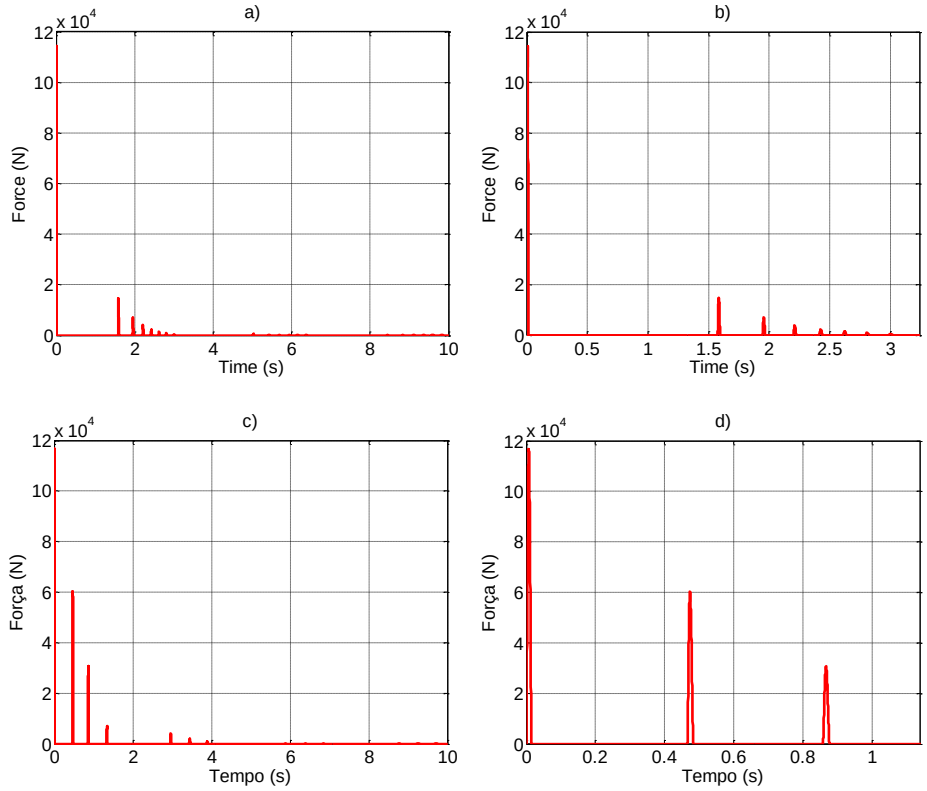

Figure 9. Contact force between mass *m* and wall *A* in models (i) and (ii) for *m* = 1000 kg. a) Contact force of model (i) for 10 s of simulation. b) Detail of contact force of model (i) for the main effective impacts (3.25 s of simulation time). c) Contact force of model (ii) for 10 s of simulation. d) Detail of contact force of model (ii) for the main effective impacts (1.15 s of simulation time).

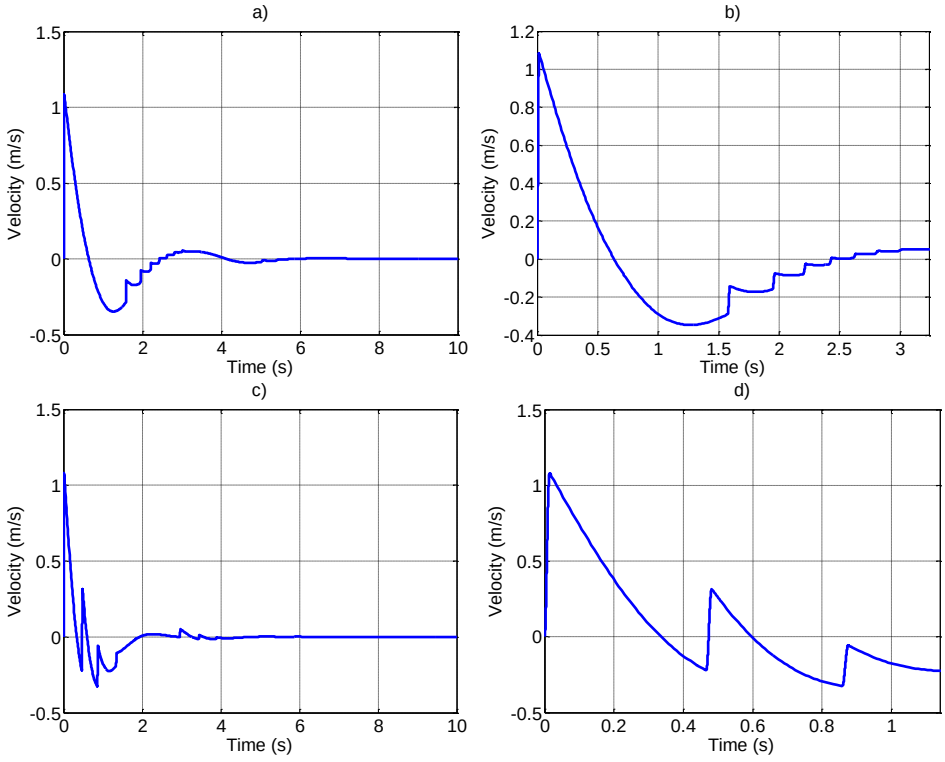

Figure 10. Velocity of mass *m* in models (i) and (ii) for *m* = 1000 kg. a) Velocity of mass *m* in models (i) for 10 s of simulation. b) Detail of velocity of mass *m* of model (i) for the main effective impacts. c) Velocity of mass *m* of model (ii) for 10 s of simulation. d) Detail of velocity of mass *m* of model (ii) for the main effective impacts.

peaks of the impact force of model (ii), as one can see comparing Fig. 9a) and Fig. 9c), or in details in Fig. 9b) and Fig. 9d).

Figure 10 shows how velocity of mass *m* varies along the simulations for model (i) and (ii). Figure 10a) presents how velocity distribution of mass m for simulation of 10 s is when we consider model (i) and Fig. 10b) is a detailed approach similar to simulation in Fig. 9b). The profile velocity of mass *m* for model (ii) for 10s of simulation is presented in Fig. 10c) and its detailed view is shown in Fig10d).

Comparing maximum velocities, both models yield practically the same. For model (i) we have a value of 1.082 m/s and for model (ii) we have 1.079 m/s of maximum velocity. Both of these velocities are considered the initial velocities of mass *m* for model (i) and model (ii), respectively. In model (i), maximum velocity occurs in 0.01484 s and the time until model (ii) reaches the maximum velocity is 0. 01495 s, i.e., a negligible difference. These values of time are practically the same as the duration of contact force, as one can verify in Fig. 11.

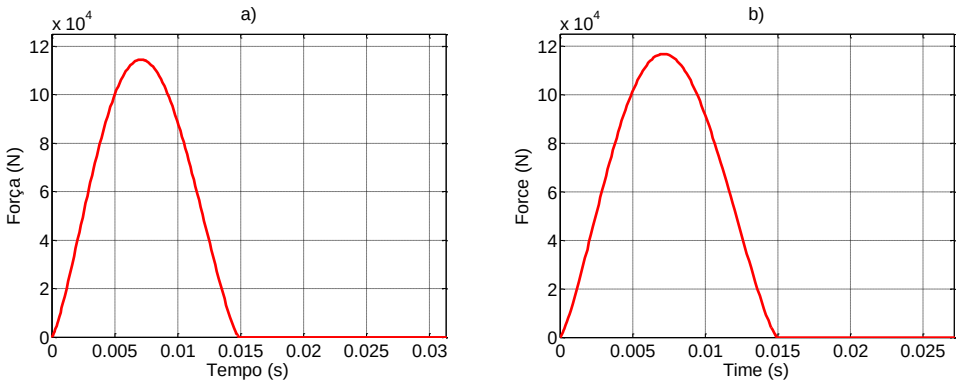

Figure 11. Maximum contact force between mass *m* and wall *A* in a) models (i) and b) model (ii).

3. CONCLUSIONS

The new proposed models are intended to improve the maximum displacement of mass *M* by the reduction of its displacement and we can observe this really happens.

For a small value of mass *m*, 100 kg, model (i) has practically the same maximum displacement of mass *M* of the Simplified Model (the maximum displacement of mass *M* in model (i) is 0.2163 m and the maximum displacement of mass *M* in the simplified model is 0.2215 m), whereas the maximum displacement of mass *M* in model (ii) is absolutely the same.

As mass *m* increases, both model (i) and model (ii) show a decrease in the maximum displacement of mass *M* as can be seen in Fig. 7 and Fig. 8.

It is well known the mass *m* acts to decrease the maximum displacement of mass *M*. The Contact Force Analysis Section explains exactly how this works by developing the impacts between mass *m* and the wall *A* and also developing the velocities profiles of mass *m*. One can observe in Fig. 9a) and in Fig. 9c) the contact force of model (i) and model (ii) respectively. One can verify both first peaks are very similar. However, the next impacts of model (i) happens after 1.5 s of the initial impact and with an amplitude much smaller than model (ii), which happens with less than 0.5 s after the first impact of mass *m.* The larger amplitude of the second impact in model (ii) has the effect of varying much more mass *m* velocity (Fig. 10c)) than in model (i) (Fig. 10a)). In conclusion, mass *m* "works" much more in model (ii) than in model (i), i. e., the absorption of energy of mass *m* in model (ii) is higher than in model (i).

Finally, besides so many differences in model (i) and model (ii), the initial velocity in both models are very similar once the first contact force is practically the same, as can be verified in Fig. 11a) and Fig. 11b).

4. ACKNOWLEDGEMENTS

The authors thank to Coordenação de Aperfeiçoamento de Pessoal de Nível Superior (CAPES), Pontifical Catholic University of Rio de Janeiro (Brazil) and Military Institute of Engineering (Brazil).

5. REFERENCES

Aguiar, R. R., 2006. *Desenvolvimento de um Dispositivo Gerador de Vibro-impacto*. Ph.D. thesis, Pontifical Catholic University of Rio de Janeiro, Brazil.

Hallenberg, A., 2006. "World War II: A Student Encyclopedia". *Reference & User Services Quarterly*, v. 45, n. 3, p. 265-267.

Hassaan, G. A., 2014a. "Dynamics of a Cannon Barrel-Recoil Mechanism with Nonlinear Air-Springs". *International Journal of Innovation and Applied Studies*, v. 8, n. 4, p. 1669.

Hassaan, G. A., 2014b. "Dynamics of a Cannon Barrel-Recoil Mechanism with a Nonlinear Hydraulic Damper". *International Journal of Modern Sciences and Engineering Technology (IJMSET)*, p. 82.

Hassaan, G. A., 2014c. "On Dynamics of a Cannon Barrel-Recoil Mechanism with Nonlinear Hydraulic Damper and Air-Springs". *International Journal of Research in Information Technology*, v. 2, n. 9, p. 704-714.

Hunt, K. H.; Crossley, F. R. E., 1968. "Coefcient of restitution interpreted as damping in vibroimpact". *Journal of Applied Mechanics - Transactions of the ASME*, p. 440 to 445, June.

Lin, T. Y., Ping, H. C., Yang, T. Y., Chan, C. T. and Yang C. C., 2009. "Dynamic simulation of the recoil mechanism on artillery weapons". In: *ICCES: International Conference on Computational & Experimental Engineering and Sciences*, p. 115-122.

Polach, P., Hajžman, M., 2010. "Design of the hydraulic shock absorbers characteristics using relative springs deflections at general excitation of the bus wheels". *Applied and Computational Mechanics*, v. 4, p. 201–214.

Tiwari, N. Patil, M. Shankar, R. Saraswat, A. and Dwivedi, R., 2016. "Rigid body dynamics modeling, experimental characterization, and performance analysis of a howitze", *Defence Technology*.

6. RESPONSIBILITY NOTICE

The authors are the only responsible for the printed material included in this paper.